Ocean Modelling 61 (2013) 38–48

Contents lists available at SciVerse ScienceDirect

Ocean Modelling

journal homepage: www.elsevier.com/locate/ocemod

Tide-surge-wave modelling and forecasting in the Mediterranean Sea with focus on the Italian coast

Christian Ferrarin [a,b,*], Aron Roland [c], Marco Bajo [a], Georg Umgiesser [a,d], Andrea Cucco [b], Silvio Davolio [e], Andrea Buzzi [e], Piero Malguzzi [e], Oxana Drofa [e]

[a] CNR – National Research Council of Italy, ISMAR – Marine Sciences Institute in Venice, Castello 2737/f, 30122 Venice, Italy
[b] CNR – National Research Council of Italy, IAMC – Institute for the Coastal Marine Environment in Oristano, 090782 Torregrande, Oristano, Italy
[c] Darmstadt University of Technology, Institute for Hydraulic and Water Resources Engineering, Darmstadt, Germany
[d] Coastal Research and Planning Institute, CORPI, Klaipėda University, H. Manto 84, 92294 Klaipėda, Lithuania
[e] CNR - National Research Council of Italy, ISAC - Institute of Atmospheric Sciences and Climate in Bologna, Via Gobetti 101, 40129 Bologna, Italy

ARTICLE INFO

Article history:
Received 30 December 2011
Received in revised form 10 September 2012
Accepted 17 October 2012
Available online 10 November 2012

Keywords:
Tide-wave-surge
Mediterranean Sea
Finite element model
Kassandra forecast system

ABSTRACT

A tide-surge-wave modelling system, called Kassandra, was developed for the Mediterranean Sea. It consists of a 3-D finite element hydrodynamic model (SHYFEM), including a tidal model and a third generation finite element spectral wave model (WWMII) coupled to the hydrodynamic model. The numerical grid of the hydrodynamic and wave models covers the whole Mediterranean with variable resolution. The comparison with coastal tide gauge stations along the Italian peninsula results in a root sum square error for the main tidal components equal to 1.44 cm. The operational implementation of the Kassandra storm surge system through the use of a high resolution meteorological model chain (GFS, BOLAM, MOLOCH) allows accurate forecast of total water level and wave characteristics. The root mean square error for the first day of forecast is 5 cm for the total water level and 22 cm for the significant wave height. Simulation results indicate that the use of a 3-D approach with a depth-varying loading factor and the inclusion of the non-linear interaction between tides and surge improve significantly the model performance in the Italian coast.

1. Introduction

Several authors (Kim et al., 2008; Brown and Wolf, 2009; Roland et al., 2009; Wolf, 2009) have shown that the coupling of wave, surge and tide is a key element to improve the accuracy of total water level coastal prediction. At the same time, accurate wave forecasting in coastal waters, where the wave field is remarkably influenced by time varying depths and currents, is only possible through a two-way coupling with a hydrodynamic model.

Simulation of storm surge and of the principal physical processes affecting coastal areas requires the use of both numerical models at high spatial and temporal resolution and downscaling techniques capable of reproducing mass exchange between the open sea and coastal waters (Xing et al., 2011). This goal can be achieved through implementation of either nested numerical models based on regular and curvilinear spatial grids (Oddo et al., 2006; Kim et al., 2008; Brown and Wolf, 2009; Debreu et al., 2012), and or numerical models based on unstructured grids Walters, 2006; Jones and Davies, 2008b; Zhang and Baptista, 2008; Roland et al., 2009; Lane et al., 2009; Xing et al., 2011.

The north Adriatic Sea is the Mediterranean sub-basin where storm surges reach higher values (Marcos et al., 2009). For this reason and also because of the presence of the city of Venice, in this area storm surges have been investigated and modelled since the 1970s (Sguazzero et al., 1972; de Vries et al., 1995). Presently, an ensemble of different statistical and deterministic models is operationally used for daily forecasts of the water level in Venice Lionello et al., 2006; Bajo et al., 2007; Bajo and Umgiesser, 2010. However, all these models do not include interactions with waves and/or tides. Climatological studies suggest that in the 21st century the storm surge frequency and magnitude in the Mediterranean Sea will progressively decrease (Marcos et al., 2011; Bellafiore et al., 2011). On the other hand the expected sea level rise will flush in the opposite direction. Exact quantifications in this aspect are not yet foreseeable. Both for this reason and because we are necessarily interested in the present times, we steadily aim at improving the accuracy of the total water level forecast.

* Corresponding author at: CNR – National Research Council of Italy, ISMAR – Marine Sciences Institute in Venice, Castello 2737/f, 30122 Venice, Italy. Tel.: +39 041 2407932; fax: +39 041 2407930.

E-mail addresses: c.ferrarin@ismar.cnr.it (C. Ferrarin), aaronroland@gmx.de (A. Roland), m.bajo@ismar.cnr.it (M. Bajo), g.umgiesser@ismar.cnr.it (G. Umgiesser), andrea.cucco@cnr.it (A. Cucco), s.davolio@isac.cnr.it (S. Davolio), a.buzzi@isac.cnr.it (A. Buzzi), p.malguzzi@isac.cnr.it (P. Malguzzi), o.drofa@isac.cnr.it (O. Drofa).

1463-5003
http://dx.doi.org/10.1016/j.ocemod.2012.10.003

The tidal oscillation in the Mediterranean Sea is generally of the order of few cm, except for the north Adriatic Sea, the north Aegean Sea and the Gulf of Gabes (Tsimplis et al., 1995).

The aim of this study is to investigate and forecast tides, storm surges and waves in the Mediterranean Sea through an unstructured-grid modelling system. Tidal model performance was evaluated against a three year long observational database of water levels acquired in the Italian coast. The accuracy of the operational model was evaluated comparing the modelled water level and wave characteristics against the corresponding measurements taken along the Italian peninsula over a one-year period.

The model chain, called Kassandra, consists of a finite-element 3-D hydrodynamic model (SHYFEM), that includes an astronomical tidal model, coupled with a finite element spectral wind wave model (WWMII). The principal forcing for the wave and hydrodynamic models is the wind at the sea surface. It is well known Wakelin and Proctor, 2002; Zampato et al., 2007; Ardhuin et al., 2007; Cavaleri et al., 2010 that, due to the complicated bordering orography, high-resolution atmospheric modelling is required to properly simulate and forecast wind fields in the Adriatic Sea. To implement an accurate forecasting system, meteorological fields are supplied by the BOLAM and MOLOCH limited-area, high-resolution models, developed and implemented at ISAC-CNR (Institute of Atmospheric Sciences and Climate – National Research Council of Italy) with a daily operational chain, using GFS (NOAA/NCEP) initial analyses and forecast lateral boundary conditions.

The short term (four days) forecasts for the Mediterranean Sea of the storm surge system are available at http://www.ismar.cnr.it/kassandra. The corresponding meteorological model products used as input of the marine model component are available at http://www.isac.cnr.it/dinamica/projects/forecasts.

2. The modelling system

The system discusses here is a coupled wave, current and astronomical-tide model using the same computational grid for all the processes. Forecast 10 m wind and atmospheric pressure fields are provided by the high resolution meteorological models BOLAM and MOLOCH described in more detail in Section 2.3.

The application of triangular unstructured grids in both the hydrodynamic and wave models has the advantage of describing more accurately complicated bathymetry and irregular boundaries in shallow water areas. It can also solve the combined large-scale oceanic and small-scale coastal dynamics in the same discrete domain by subdivision of the basin in triangles varying in form and size.

The considered interactions between waves, surge and tides are: (1) the contribution of waves to the total water levels by mean of the wave set-up and wave set-down; (2) the influence of tides and storm surge on the wave propagation affecting the refraction, shoaling and breaking processes; (3) the effect of water level variation and currents on the propagation, generation and decay of the wind waves.

The spatial variation of the wave action spectra causes a net momentum flux known as radiation stress (Longuet-Higgins and Steward, 1964). The onshore component of this momentum flux is balanced by a pressure gradient in the opposite direction. The physical manifestation of this pressure gradient is the rise or fall of the mean sea level, known as wave set-up and wave set-down respectively. Especially during storm conditions, the radiation stress can be an important terms in storm surge applications as wave set-up increases the water level close to the coast causing widespread damages associated with flooding of the coastal areas (Brown et al., 2011).

The influence of the wave dependent ocean surface roughness on the wind stress parameterization Øyvind et al., 2007; Moon et al., 2009; Olabarrieta et al., 2012; Bertin et al., 2012; Bolaños et al., 2011 and the increase of the bottom friction due to the presence of a wave boundary layer (e.g.Grant and Madsen, 1979) are not considered in this study and will be investigated in a future version of the modelling system.

2.1. The hydrodynamic model

The 3-D hydrodynamic model SHYFEM here applied uses finite elements for horizontal spatial integration and a semi-implicit algorithm for integration in time (Umgiesser and Bergamasco, 1995; Umgiesser et al., 2004).

The primitive equations, vertically integrated over each layer, are:

$$\begin{aligned}&\frac{\partial U_l}{\partial t}+u_l\frac{\partial U_l}{\partial x}+v_l\frac{\partial U_l}{\partial y}-fV_l\\&\quad=-gh_l\frac{\partial\zeta}{\partial x}-\frac{gh_l}{\rho_0}\frac{\partial}{\partial x}\int_{-H_l}^{\zeta}\rho' dz-\frac{h_l}{\rho_0}\frac{\partial p_a}{\partial x}+\frac{1}{\rho_0}\left(\tau_x^{top(l)}-\tau_x^{bottom(l)}\right)\\&\qquad+\frac{\partial}{\partial x}\left(A_H\frac{\partial U_l}{\partial x}\right)+\frac{\partial}{\partial y}\left(A_H\frac{\partial U_l}{\partial y}\right)+\frac{F_l^x}{\rho h_l}+gh_l\frac{\partial\eta}{\partial x}-gh_l\beta\frac{\partial\zeta}{\partial x}\end{aligned}\tag{1a}$$

$$\begin{aligned}&\frac{\partial V_l}{\partial t}+u_l\frac{\partial V_l}{\partial x}+v_l\frac{\partial V_l}{\partial y}+fU_l\\&\quad=-gh_l\frac{\partial\zeta}{\partial y}-\frac{gh_l}{\rho_0}\frac{\partial}{\partial y}\int_{-H_l}^{\zeta}\rho' dz-\frac{h_l}{\rho_0}\frac{\partial p_a}{\partial y}\\&\qquad+\frac{1}{\rho_0}\left(\tau_y^{top(l)}-\tau_y^{bottom(l)}\right)+\frac{\partial}{\partial x}\left(A_H\frac{\partial V_l}{\partial x}\right)+\frac{\partial}{\partial y}\left(A_H\frac{\partial V_l}{\partial y}\right)\\&\qquad+\frac{F_l^y}{\rho h_l}+gh_l\frac{\partial\eta}{\partial y}-gh_l\beta\frac{\partial\zeta}{\partial y}\end{aligned}\tag{1b}$$

$$\frac{\partial\zeta}{\partial t}+\sum_l\frac{\partial U_l}{\partial x}+\sum_l\frac{\partial V_l}{\partial y}=0\tag{1c}$$

with l indicating the vertical layer, (U_l, V_l) the horizontal transport at each layer (integrated velocities), f the Coriolis parameter, p_a the atmospheric pressure, g the gravitational acceleration, ζ the sea level, ρ_0 the average density of sea water, $\rho=\rho_0+\rho'$ the water density, τ the internal stress term at the top and bottom of each layer, h_l the layer thickness, H_l the depth at the bottom of layer l. Smagorinsky's formulation (Smagorinsky, 1963; Blumberg and Mellor, 1987) is used to parameterize the horizontal eddy viscosity (A_h). For the computation of the vertical viscosities a turbulence closure scheme was used. This scheme is an adaptation of the k-ϵ module of GOTM (General Ocean Turbulence Model) described in Burchard and Petersen, 1999.

The coupling of wave and current models was achieved through the gradients of the radiation stress induced by waves (F_l^x and F_l^y) computed using the theory of Longuet-Higgins and Steward (1964). The vertical variation of the radiation stress was accounted following the theory of Xia et al. (2004). The shear component of this momentum flux along with the pressure gradient creates second-order currents.

The model calculates equilibrium tidal potential (η) and load tides and uses these to force the free surface (Kantha, 1995). The term η in Eqs. 1a and 1b, is calculated as a sum of the tidal potential of each tidal constituents multiplied by the frequency-dependent elasticity factor (Kantha and Clayson, 2000). The factor β accounts for the effect of the load tides, assuming that loading tides are in-phase with the oceanic tide (Kantha, 1995). Four semi-diurnal (M2, S2, N2, K2), four diurnal (K1, O1, P1, Q1) and four long-term constituents (Mf, Mm, Ssa, MSm) are considered by the model.

Velocities are computed in the center of the grid element, whereas scalars are computed at the nodes. Vertically the model applies Z layers with varying thickness. Most variables are computed in the center of each layer, whereas stress terms and vertical velocities are solved at the interfaces between layers. The

horizontal diffusion and the advective terms in the momentum equation are treated explicitly. The Coriolis force, the barotropic pressure gradient terms in the momentum equation and the divergence term in the continuity equation are treated semi-implicitly. The vertical stress terms and the bottom friction term are treated fully implicitly for stability reasons in the very shallow parts of the domain. The discretization results in unconditional stability which is essential for modelling the effects of fast gravity waves, bottom friction and the Coriolis acceleration (Umgiesser and Bergamasco, 1995).

The boundary conditions for stress terms are:

$$\tau_x^{surface} = c_D \rho_a w_x \sqrt{u_w^2 + v_w^2} \quad \tau_y^{surface} = c_D \rho_a w_y \sqrt{u_w^2 + v_w^2} \tag{2a}$$

$$\tau_x^{bottom} = c_B \rho_0 u_L \sqrt{u_L^2 + v_L^2} \tau_y^{bottom} = c_B \rho_0 v_L \sqrt{u_L^2 + v_L^2} \tag{2b}$$

where c_D is the wind drag coefficient, c_B is the bottom friction coefficient, ρ_a is the air density, u_w and v_w are the zonal and meridional components of the wind velocity respectively, u_L and v_L are the water velocities in the bottom layer.

2.2. The wind wave model

WWMII is a third generation spectral wind wave model, which uses triangular elements in geographical space to solve the Wave Action Equation (WAE) (Roland et al., 2009). In Cartesian coordinates, the WAE reads as follows:

$$\underbrace{\frac{\partial}{\partial t} N}_{\text{Change in time}} + \underbrace{\nabla_{\mathbf{x}} (c_{\mathbf{x}} N)}_{\text{Advection in geographical space}} + \underbrace{\frac{\partial}{\partial \sigma}(c_\sigma N) + \frac{\partial}{\partial \theta}(c_\theta N)}_{\text{Intra-spectral propagation}} = \underbrace{S_{tot}}_{\text{Total source term}} \tag{3}$$

where $N = N(t, x, y, \sigma, \theta)$ is the wave action density spectrum, t is the time, $\mathbf{X} = (x, y)$ is the coordinate vector in geographical space, $c_{\mathbf{x}}$ is the wave propagation velocity vector, c_σ and c_θ are the wave propagation velocities in σ and θ space, respectively; σ is the relative frequency and θ is the wave direction.

The WAE describes the evolution of wind waves in slowly varying media. In this work the wave model is coupled to the hydrodynamic model to account for wave refraction and shoaling induced by variable depths and currents. The propagation velocities in the different phase spaces are defined as:

$$c_{\mathbf{x}} = c_g + \mathbf{U} \tag{4a}$$

$$c_\theta = \frac{1}{k} \frac{\partial \sigma}{\partial H} \frac{\partial H}{\partial m} + \mathbf{k} \frac{\partial \mathbf{U}}{\partial s} \tag{4b}$$

$$c_\sigma = \frac{\partial \sigma}{\partial H} \left(\frac{\partial H}{\partial t} + U_A \cdot \nabla_{\mathbf{x}} H \right) - c_g \mathbf{k} \frac{\partial \mathbf{U}}{\partial s} \tag{4c}$$

where $\mathbf{U}$ is the velocity vector of the fluid (we use surface current velocity in deep water and depth average current velocity in shallow water), s and m are the directions along wave propagation and perpendicular to it, $\mathbf{k} = (k_x, k_y)$ is the wave number vector and k is its magnitude, c_g is the group velocity and H is the water depth.

The model solves the geographical advection by using the family of so called residual distributions schemes, while the spectral part is solved using ultimate quickest schemes (Tolman, 1991).

The term S_{tot} in the right-hand side of Eq. (3) is the source function which includes the energy input due to wind (S_{in}), the non-linear interaction in deep and shallow water (S_{nl4} and S_{nl3}), the energy dissipation due to whitecapping and depth induced wave breaking (S_{ds} and S_{br}) and the energy dissipation due to bottom friction (S_{bf}):

$$S_{tot} = \underbrace{S_{in} + S_{nl4} + S_{ds}}_{\text{Deep water source terms}} + \underbrace{S_{nl3} + S_{br} + S_{bf}}_{\text{Shallow water source terms}} \tag{5}$$

The non-linear terms S_{nl4} and S_{nl3} are evaluated with the discrete interaction approximation (DIA) (Hasselmann and Hasselmann, 1981) and the lumped triad approximation (LTA) (Eldeberky, 1996) respectively. The dissipation formulation for bottom friction is based on the empirical JONSWAP model by Hasselmann et al. (1973) with a constant dissipation coefficient of −0.067. For the depth-induced wave breaking, the formulation of Battjes and Janssen (1978) was implemented. The wind input function and whitecapping dissipation function are based on the formulation of Makin and Stam (2003). In conditions when the waves run opposite to the wind direction the formulation by Young and Sobey (1985) was used. The corresponding dissipation function has been formulated according to Makin and Stam (2003).

2.3. The meteorological models

At the ISAC-CNR (Italy) a numerical weather prediction chain is implemented. The model framework comprises the hydrostatic model BOLAM and the non-hydrostatic model MOLOCH, nested in BOLAM. The initial and boundary conditions are derived from the analyses (00 UTC) and forecasts of the GFS (NOAA/NCEP, USA) global model http://www.emc.ncep.noaa.gov/GFS.

BOLAM is operated with a horizontal grid spacing of 0.10 deg in rotated coordinates (spatial resolution about 11 km), with 50 vertical levels. Moist deep convection is parameterized using the Kain–Fritsch convective scheme, updated on the basis of the revision proposed by Kain (2004) and completely recoded imposing conservation of liquid water static energy. Moreover, additional modifications with respect to the Kain, 2004 version were introduced in order to stabilize a little more efficiently the lower troposphere. The BOLAM model provides forecasts up to 3 days in advance over a domain which comprises Europe and the whole Mediterranean Sea.

The non-hydrostatic MOLOCH model has a horizontal grid spacing of 0.021 deg, corresponding to 2.3 km, with 54 vertical levels. Moist deep convection is computed explicitly using direct simulation of the microphysical processes (Drofa and Malguzzi, 2004). MOLOCH forecasts are provided up to 48 h over Italy. See Buzzi et al., 1994; Malguzzi et al., 2006 and Richard et al., 2007 for further details about the BOLAM and MOLOCH models.

The BOLAM and MOLOCH data (namely 10 m wind and mean sea level pressure) is made available at hourly frequency for the duration of the respective forecast intervals, starting at 00 UTC of each day (03 for MOLOCH), on the original model grids. Such meteorological forcing are then interpolated on the finite element marine models grid. For the first two days of forecast the interpolated fields are obtained combining the MOLOCH data over the Italian peninsula and the BOLAM data for the remaining Mediterranean region. The BOLAM model provides all data for the third day of forecast. The GFS data (available at 0.5 deg resolution) is used to force the oceanographic model during the fourth day of forecast.

2.4. Model set-up

The hydrodynamic and wave numerical computation is performed on a spatial domain that represents the Mediterranean Sea by means of an unstructured grid. The use of elements of variable sizes, typical of finite element methods, is fully exploited, in order to suit the complicated geometry of the basin, the rapidly varying topographic features, and the complex bathymetry.

The numerical grid used by the hydrodynamic and the wave model covers the whole Mediterranean with approximately 140,000 triangular elements and a resolution that varies from 15 km in the open sea to 5 km in coastal waters and less than 1 km on the coasts of Italy (Fig. 1). The 1-min resolution GEBCO

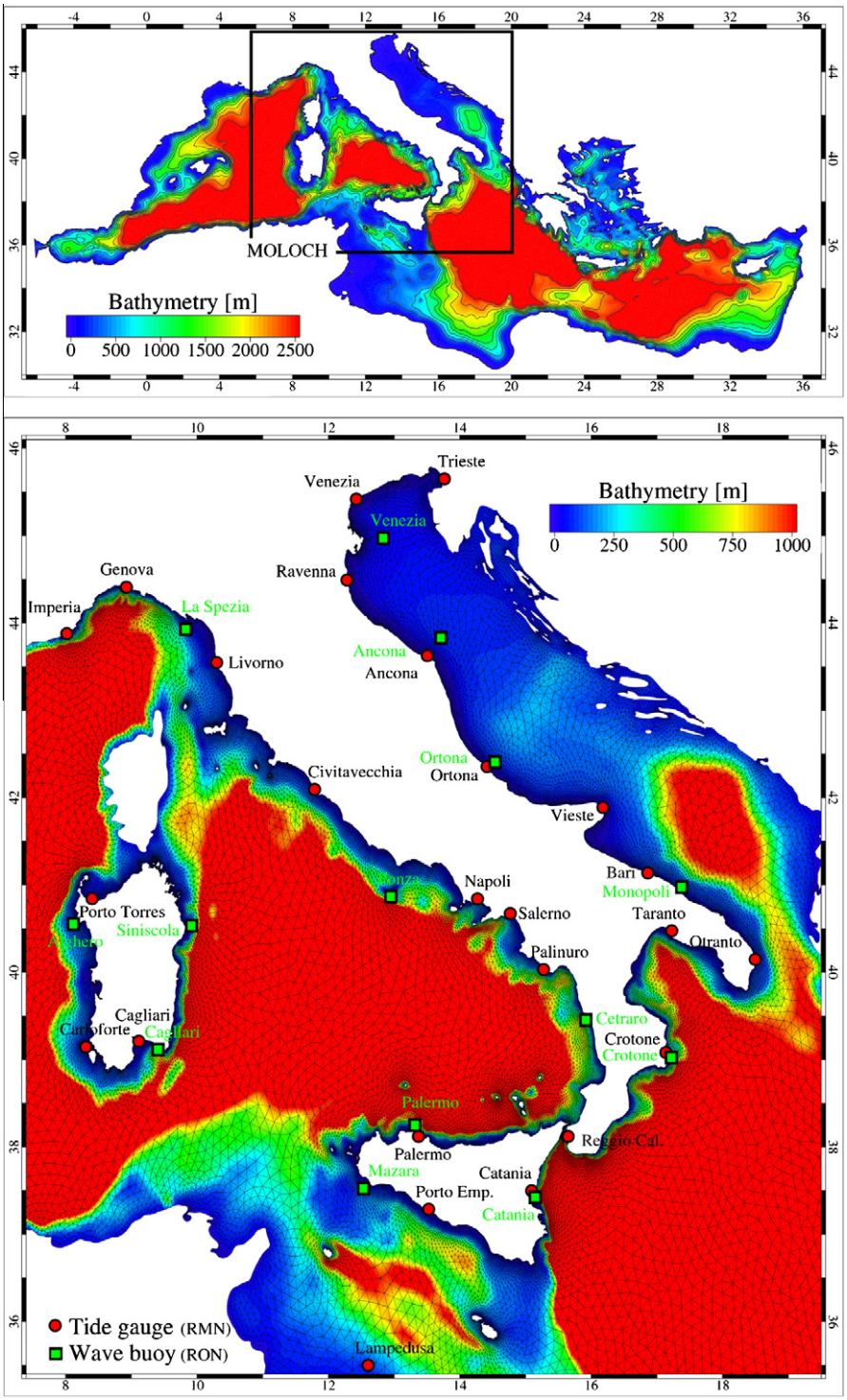

Fig. 1. Hydrodynamic and wave models domain and bathymetry. The bottom panel shows a detailed view of the numerical grid around the Italian peninsula. Circles mark the location of the tidal gauges and squares indicate the location of the wave buoys. The black rectangle in the upper panel represents the spatial coverage of the MOLOCH atmospheric model.

(the general bathymetric charts of the oceans) bathymetric data is interpolated on the finite element mesh.

The hydrodynamic model is applied in its 3-D version. The water column is discretized into 16 vertical levels with progressively increasing thickness varying from 2 m for the first 10 m to 500 m for the deepest layer, beyond the continental shelf. The drag coefficient for the momentum transfer of wind in the hydrodynamic model (c_D) is set following Smith and Banke, 1975.

The astronomical tide calculated by the global FES2004 model (Lyard et al., 2006) is imposed to the hydrodynamic model as boundary condition at the Strait of Gibraltar. Baroclinic terms, river input and heat fluxes are not considered and no data assimilation is performed in the modelling system.

The wave model, which at this stage is parallelized using OpenMP, represents the most computationally expensive part of the forecast system. For the wave model integration, nine computer

processors are used and therefore we have adopted 18 wave frequencies, ranging from 0.04 to 1.0 Hz, and 18 uniformly wave distributed directions. We are aware of the poor scaling of such setting for the S_{nl4}.

3. Results and discussion

This section is organized in two main parts: the first describes the hindcast modelling results and the second presents the results of the short term forecast system for the total water level and the significant wave height.

The accuracy of the model is evaluated by comparing the predicted water level and significant wave height with observations collected along the Italian coast. The Italian observational system is administrated by the Italian Institute for Environmental Protection and Research (ISPRA) and consists of 25 coastal tidal gauges (circles in Fig. 1, http://www.mareografico.it) and 15 coastal wave buoys (squares in Fig. 1, http://www.telemisura.it).

3.1. Hindcast modelling

A five year-long hindcast simulation (2005–2009) was performed to evaluate model performance. The spin-up period of this simulation was 2 years.

3.1.1. Tidal model validation

Time series of available data and model results were analysed with the TAPPY tidal analysis package (Cera, 2011). The observed database consists of three year-long (2007–2009) hourly records from the tidal gauges located around the Italian peninsula (circles in Fig. 1).

The model performance was assessed by calculating the vectorial differences for each of the diurnal and semi-diurnal constituents:

$$d_{i,j} = \sqrt{(a^o_{i,j}cosg^o_{i,j} - a^m_{i,j}cosg^m_{i,j})^2 + (a^o_{i,j}sing^o_{i,j} - a^m_{i,j}sing^m_{i,j})^2} \quad (6)$$

where a = amplitude (cm), g = phase (degrees), subscript i refers to the tidal gauge station, subscript j refers to the tidal constituent, superscript o is the observed data from the tide gauge and superscript m is the model result (Foreman et al., 1993; Tsimplis et al., 1995).

For each tidal constituent j the root mean square deviation of amplitude (RMS) is defined as follows:

$$RMS_j = \sqrt{\frac{1}{2N}\sum_{i=1}^{N} d^2_{i,j}} \quad (7)$$

where N is the number of tide gauges considered and $d_{i,j}$ is the vectorial difference defined in Eq. 6 for each location i.

Furthermore the root sum of squares (RSS) was computed, which accounts for the total effect of the n major tide constituents for each model against the tide-gauge observations (Arabelos et al., 2010). RSS is defined as:

$$RSS = \sqrt{\sum_{j=1}^{n} RMS^2_j} \quad (8)$$

Several numerical tests were carried out to investigate the effect of different approximations and processes. Results of the different simulations are represented in Fig. 2 in terms of RMS and RSS, computed over all 25 tide gauge sites. The base experiment, which was based on 2-D approach without considering both loading tide and tide-surge interaction, had a RSS of 2.09 cm. As shown in Fig. 2, RMS is larger than 1 for the M2 and K1 tidal constituents.

Even if we are dealing only with barotropic forcing and we assume unstratified water, the use of the 3-D approach reduced RSS 1.92 cm. This is due to the fact that the bottom stress differs in the two cases: in 2-D model it is based on depth-averaged velocity, whereas in the 3-D case it depends on the near-bottom velocity. Weisberg and Zheng (2008) suggested that three-dimensional models are preferable over two-dimensional models for simulating storm surges.

The effect of ocean self-attraction and loading is accounted by the factor β in the dynamical equations (Eq. 1a and 1b). The global average value of this parameter is $\beta = 0.12 \pm 0.05$ (Stepanov and Hughes, 2004). The coefficient in the open sea is larger than near the coast since the characteristic length scale for tidal motions decreases in shallow water (Stepanov and Hughes, 2004). Numerical experiments were carried out using constant and depth-varying β factor. The results of these experiments (Fig. 2) demonstrated that along the Italian peninsula using a loading tide factor linearly dependent on depth $\beta = \alpha H$, with α a calibration parameter equal to $7{\cdot}10^{-5}$, reduced RSS from 1.77 to 1.54 cm.

A last numerical hindcast experiment was performed forcing the 3-D barotropic model with depth-varying β factor by wind and pressure data of the years simulated. As shown in Fig. 2, RMS is larger than 0.5 cm for the M2, K1 and O1 tidal constituents.

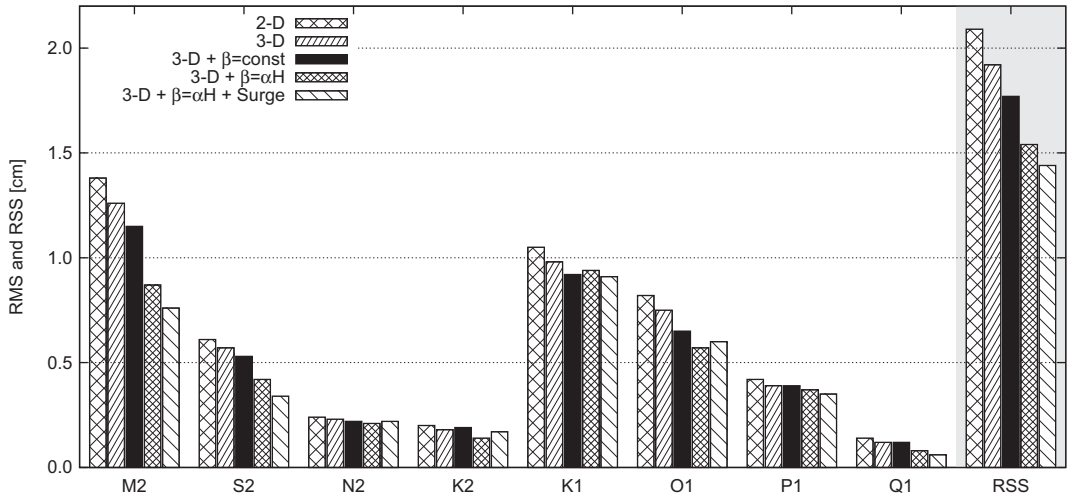

Fig. 2. RMS of principal diurnal and semi-diurnal tidal constituents and RSS for the considered numerical experiments: 2-D, 3-D, 3-D with constant β parameter, 3-D with linearly varying β parameter, 3-D with linearly varying β parameter and tide-surge interaction.

Table 1
Statistical analysis of diurnal and semi-diurnal tidal constituents at all water level monitoring stations (marked with circles in Fig. 1). Analysis results are given as vectorial differences between simulated and observed values (Eq. 6) and RMS (Eq. 7). Unit is cm. Asterisks identify the stations used in the tidal model intercomparison.

Station	*Semi-diurnal*				*Diurnal*			
	M2	S2	N2	K2	K1	O1	P1	Q1
Ancona*	0.37	0.46	0.07	0.15	1.46	1.09	0.62	0.26
Bari	1.04	0.51	0.31	0.38	0.72	0.43	0.27	0.17
Cagliari*	0.64	0.13	0.02	0.11	1.56	0.97	0.51	0.03
Carloforte*	1.10	0.34	0.23	0.11	1.89	1.08	0.65	0.06
Catania*	0.40	0.22	0.20	0.27	0.64	0.08	0.40	0.08
Civitavec.*	2.30	0.64	0.59	0.32	1.08	0.98	0.34	0.08
Crotone	0.24	0.19	0.24	0.08	0.32	0.23	0.37	0.20
Genova*	0.48	0.31	0.20	0.19	1.83	1.04	0.60	0.03
Imperia	0.62	0.35	0.20	0.12	1.57	1.06	0.60	0.03
Lampedusa*	0.61	0.64	0.17	0.40	0.56	0.51	0.25	0.05
Livorno*	1.10	0.43	0.31	0.20	2.06	1.26	0.75	0.04
Napoli*	0.37	0.26	0.13	0.06	1.20	0.94	0.52	0.04
Ortona*	1.31	0.78	0.31	0.41	1.02	0.92	0.51	0.22
Otranto*	0.55	0.56	0.16	0.20	0.72	0.55	0.27	0.13
Palermo*	0.93	0.51	0.24	0.16	1.04	0.85	0.41	0.02
Palinuro	0.36	0.06	0.03	0.03	1.44	1.02	0.61	0.03
P. Empedocle	0.29	0.07	0.24	0.42	0.29	0.22	0.17	0.10
Porto Torres	2.76	1.28	0.71	0.31	0.86	0.80	0.35	0.13
Ravenna	0.20	0.94	0.36	0.65	1.67	1.40	0.85	0.23
Reggio Cal.	1.55	0.42	0.36	0.36	1.06	0.22	0.35	0.10
Salerno	0.52	0.08	0.05	0.07	1.45	0.97	0.63	0.04
Taranto*	0.22	0.35	0.15	0.17	0.52	0.29	0.22	0.10
Trieste*	1.20	1.84	0.54	0.74	1.75	1.54	0.96	0.24
Venezia*	1.42	1.25	0.56	0.88	1.69	1.35	0.69	0.29
Vieste*	1.04	0.59	0.30	0.49	0.82	0.56	0.31	0.18
RMS	0.76	0.33	0.22	0.17	0.91	0.60	0.35	0.06

Model results (Fig. 2) demonstrated that, for the Italian coast, accounting for the non-linear interaction between tide and surge reduces RSS to 1.44 cm. Both tidal amplitude and phase are modified by the non-linear tide-surge interaction. This is due to the fact that in shallow water regions the presence of the surge influences the tidal distribution through the bottom friction and non-linear momentum advection terms (Horsburgh and Wilson, 2007; Jones and Davies, 2008a; Xing et al., 2011).

The statistics of the final set of model results for all 25 tide gauge sites and for principal diurnal and semi-diurnal constituents are reported in Table 1 and in Fig. 3. A satisfactory agreement between the computed and empirical tidal constituents is found.

Table 2
RMS and RSS misfit between observations and corresponding modelled amplitude and phases. Unit is cm.

Model	*RMS*				*RSS*
	M2	S2	K1	O1	
Kassandra	0.727	0.506	0.945	0.674	1.460
Tsimplis et al., 1995	1.278	1.027	1.393	0.328	2.176
Arabelos et al., 2010	1.340	0.745	0.977	0.849	2.006

The average vectorial difference is lower than 1 cm for all constituents except for the K1 diurnal tidal wave. The highest differences are found in the Northern Adriatic Sea, which is one of the areas with maximum tidal amplitude in the whole Mediterranean Sea.

The Kassandra model performance was compared with existing tidal models for the Mediterranean Sea. The selected tidal models used in this study, and for which results are available, are the following:

- the two-dimensional hydrodynamic model of Tsimplis et al. (1995) which is forced by the equilibrium tide and the incoming tide at the Strait of Gibraltar. The model has a regular resolution of 1/12° and considers the M2, S2, K1, and O1 tidal constituents.
- the barotropic ocean tide model of Arabelos et al., 2010 developed by assimilation of tide-gauge data and TOPEX/Poseidon data. The model grid is $2'x2'$ and the following tidal waves are modelled: M2, S2, N2, K2, K1, O1, P1, Q1.

The inter-comparison of the three models was based on comparison of constituents extracted from the observations at 16 sites along the Italian peninsula (stations marked with an asterisk in Table 1), with constituents extracted at the same points from Kassandra and the two selected regional tidal models according to previously published results. Model comparison was performed considering the tidal constituents M2, S2, K1 and O1. The results in terms of RMS and RSS are shown in Table 2.

Inspection of Table 2 indicates that along the Italian peninsula and for the period considered the Kassandra modelling system (RSS = 1.46 cm) has performed better than both the hydrodynamic model of Tsimplis et al. (1995) (RSS = 2.18 cm) and the assimilation based model (Table 3 in Arabelos et al. (2010)) (RSS = 2.00 cm).

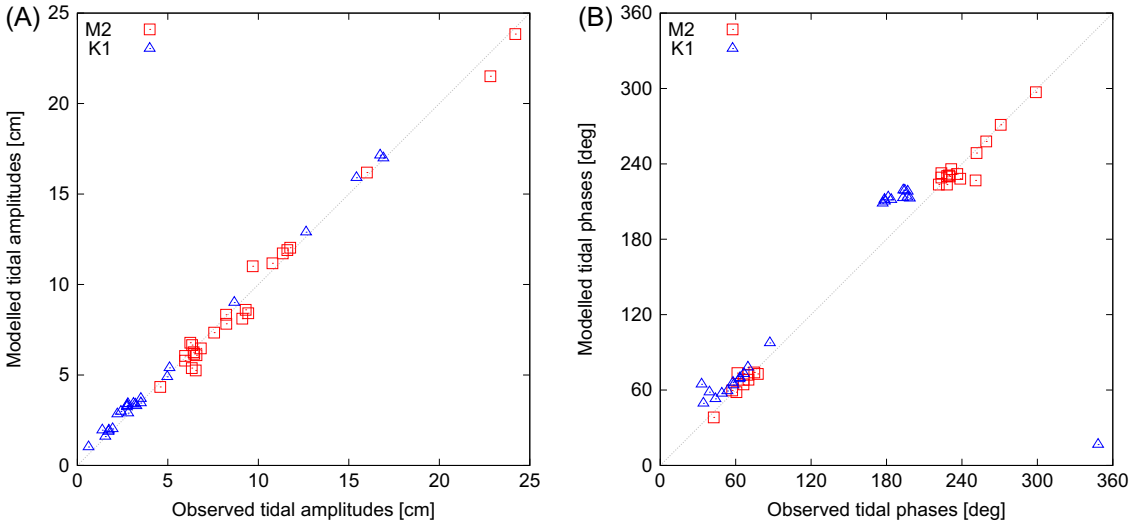

Fig. 3. Scatter plots of empirical and modelled M2 and K1 tidal amplitude (cm) and phase (deg) at 25 different coastal stations along the Italian coast.

Table 3
Statistical analysis of simulated total water level for the tidal gauges as mean of the values for the first day of forecast. The statistics (bottom lines) are reported also as mean over all stations for each of the forecast days (F1, F2, F3, F4). Analysis results are given in terms of difference between mean of the observations and simulations (BIAS), normalized standard deviation of simulations (Norm. STD), centred root mean square difference (CRMS) and correlation coefficient (Corr). Unit is cm.

Station	Bias	Norm. STD	CRMS	Corr
Ancona	−2.5	1.05	6.0	0.90
Bari	−13.9	0.91	5.0	0.89
Cagliari	17.6	0.84	5.4	0.81
Carloforte	16.5	0.73	5.5	0.81
Catania	5.8	0.96	4.9	0.77
Civitavec.	−0.0	1.03	5.1	0.86
Crotone	−14.6	0.94	4.2	0.83
Genova	8.0	0.87	5.0	0.86
Lampedusa	4.7	0.79	5.1	0.80
Livorno	0.5	0.85	5.3	0.86
Napoli	−10.9	1.01	4.6	0.90
Ortona	−2.9	0.99	5.8	0.86
Otranto	−23.4	1.00	4.1	0.86
Palermo	8.9	0.96	5.4	0.85
Palinuro	−8.1	1.00	4.4	0.91
Porto Torres	18.8	0.79	4.9	0.84
Ravenna	9.2	0.98	7.0	0.94
Reggio Cal.	−14.4	0.84	5.5	0.68
Salerno	−14.9	1.00	4.7	0.89
Taranto	−18.5	0.94	4.4	0.83
Trieste	−0.2	0.93	8.0	0.96
Venezia	16.1	0.95	7.5	0.96
Vieste	−9.8	0.94	5.3	0.87
Mean F1	–	0.93	5.4	0.86
Mean F2	–	0.93	5.4	0.86
Mean F3	–	0.92	5.5	0.85
Mean F4	–	0.90	5.4	0.85

3.1.2. Hydrodynamic-wave interactions

In order to investigate the effect of wave-current interactions, the model results are compared to those obtained from the same system without considering the interactions between the tide, wave and surge (uncoupled version).

Analysis of simulation results are presented in terms of the difference between the average of observed and simulated values (BIAS), centred root mean square error (CRMS), correlation coefficient (Corr) and Scatter Index (SCI, defined as the CRMS divided by the mean of observed values).

Wave set-up occurs only in the surf zones to establish the primary momentum balance between cross-shore breaker momentum acceleration (the major component in the radiation stress divergence) and the pressure gradient force (Bowen et al., 1968). Storm surge statistics, obtained comparing the modelled and observed residual signal (total water level minus astronomical tide), of the two simulations (coupled vs. uncoupled) do not differ significantly. Thus, even if the model coupling is correctly implemented, in the present model version the discretization at the coast (about 1 km) is not enough to properly resolve this process, since generally the surf zone along the Italian coast is in the order of few hundreds meters even during storms except the coastal part of the Northern Adriatic Sea, characterized by a gentle slope. Here it was found in Roland et al. (2009), that during the "century storm" of November 1966, a wave set-up of more than 40 cm and a surf zone which extend for about 2–3 km.

The influence of varying currents and water level on the waves have been evaluated comparing the skill of the coupled and the uncoupled model versions. The statistical analysis carried out for all in situ wave buoy stations showed a weak but persistent signal of improved statistics for the significant wave height. Model results demonstrated that, for the Italian coast, accounting for the hydrodynamic-wave interactions reduced CRMS (from 0.30 to 0.29 m), BIAS (from 0.13 to 0.12 m) and SCI (0.36 to 0.35). Such a improvement, is consistent for all three statistical parameters and is considerable since it is referred to the whole period of investigation.

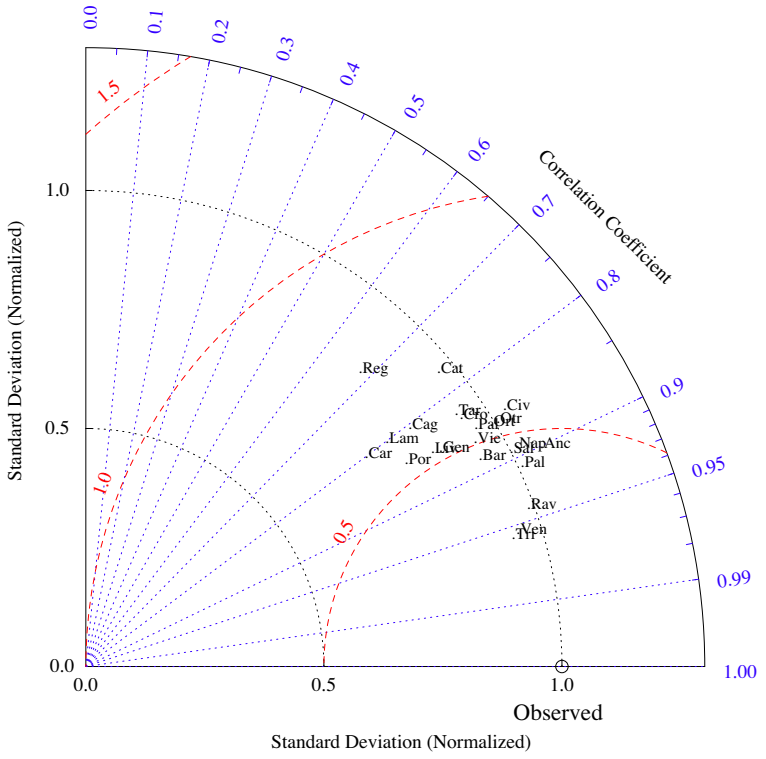

Fig. 4. Taylor diagram displaying a statistical comparison with observation of simulated total water level for the first day of forecast in all tidal gauges. The circle on the bottom axis represents the observations and the red dashed contours indicate the normalized root mean square error.

Table 4
As Table 3 but for the significant wave height. Unit is m.

Station	Bias	Norm. STD	CRMS	Corr	SCI
Alghero	0.06	0.92	0.29	0.96	0.28
Ancona	0.08	0.95	0.19	0.90	0.34
Cagliari	0.00	1.09	0.25	0.93	0.26
Catania	0.07	0.93	0.20	0.92	0.31
Cetraro	0.03	0.88	0.19	0.95	0.32
Civitavec.	0.02	1.04	0.20	0.93	0.33
Crotone	0.06	1.01	0.21	0.93	0.32
La Spezia	0.10	0.98	0.26	0.93	0.35
Mazara	0.03	0.98	0.20	0.95	0.25
Monopoli	0.03	0.96	0.20	0.91	0.34
Ortona	0.06	0.90	0.28	0.91	0.40
Palermo	0.05	0.87	0.19	0.94	0.30
Ponza	0.06	0.96	0.21	0.94	0.28
Siniscola	0.01	0.95	0.16	0.91	0.29
Venezia	0.00	1.00	0.24	0.83	0.55
Mean F1	0.04	0.96	0.22	0.92	0.33
Mean F2	0.05	0.96	0.25	0.90	0.37
Mean F3	0.10	0.90	0.28	0.87	0.42
Mean F4	0.15	0.81	0.33	0.82	0.48

3.2. Forecast modelling

The Kassandra forecasting system has been operational since February 2011, hence almost one year of model results is available at present for statistical analysis.

Model performance is graphically summarized through Taylor diagrams (Taylor, 2001). The position of each label on the graph represents a different model result and is determined by the values of the correlation coefficient and standard deviation. In the Taylor diagrams the statistics have been normalized by dividing both the centred root mean square error and the standard deviation of the model by the standard deviation of the observations. This procedure allows to plot together comparable statistical indexes for different monitoring stations and for different fields. The perfect fit between model results and data is represented by a circle mark on the x-axis at unit distance from the origin.

The statistics of the simulated water level are reported in Table 3 and plotted in Fig. 4. On average, the total water level simulated for the first forecast day has a correlation of 0.86 and a CRMS of 5.4 cm. The BIAS is highly varying along the Italian peninsula (from −24 to 18 cm) and could be partially attributed to the varying Atlantic water level and to the sea level anomalies induced by the thermohaline Mediterranean circulation which is not described by the Kassandra barotropic model.

Model skill is high spatially varying over the considered domain. Fig. 4 shows that in the Northern Adriatic Sea (stations of Ravenna, Venezia, and Trieste) the model presents the best agreement with the observations, with a correlation coefficient exceeding 0.94. These stations shows the highest correlations and the lowest normalized CRMS (divided by the amplitude of the observations variation) because the Northern Adriatic Sea is characterized by water level oscillations higher than along the other Italian coasts. The contribution of the tidal signal relative to the observed water level variance is more than 73% in the Northern Adriatic Sea, while is about 30% in the Ionian Sea (the average over the Italian peninsula is 44%).

The Kassandra modelling system is capable of producing accurate forecasts of the wave field around the Italian peninsula. The results of the statistical analysis of the simulated significant wave height of the first day of forecast are reported in Table 4 and graphically summarized by the Taylor diagram of Fig. 5. The model results compare reasonably well with the measurements, with a mean CRMS of 22 cm and a mean scatter index of 0.33 (averaged over all stations). The correlation coefficient exceeds 0.90 in most of the stations (except Venezia) and the BIAS ranges from 0 to 10 cm. Wave model performance is comparable with other existing wave forecasting systems operating in the Mediterranean Sea (Bertotti and Cavaleri, 2009; Bertotti et al., 2011).

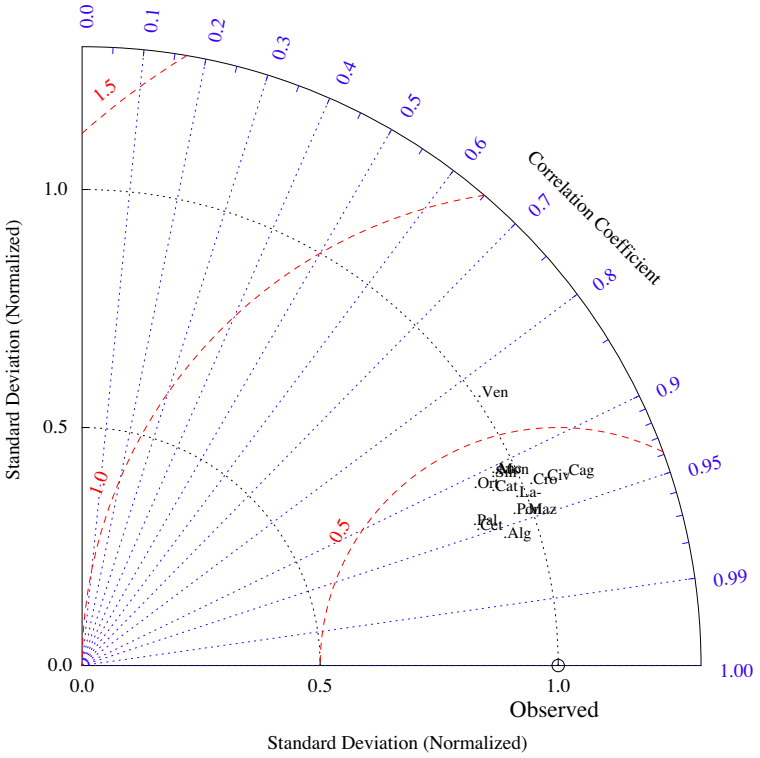

Fig. 5. Taylor diagram as Fig. 4 but displaying a statistical comparison with observation of simulated significant wave height for the first day of forecast in all wave buoys.

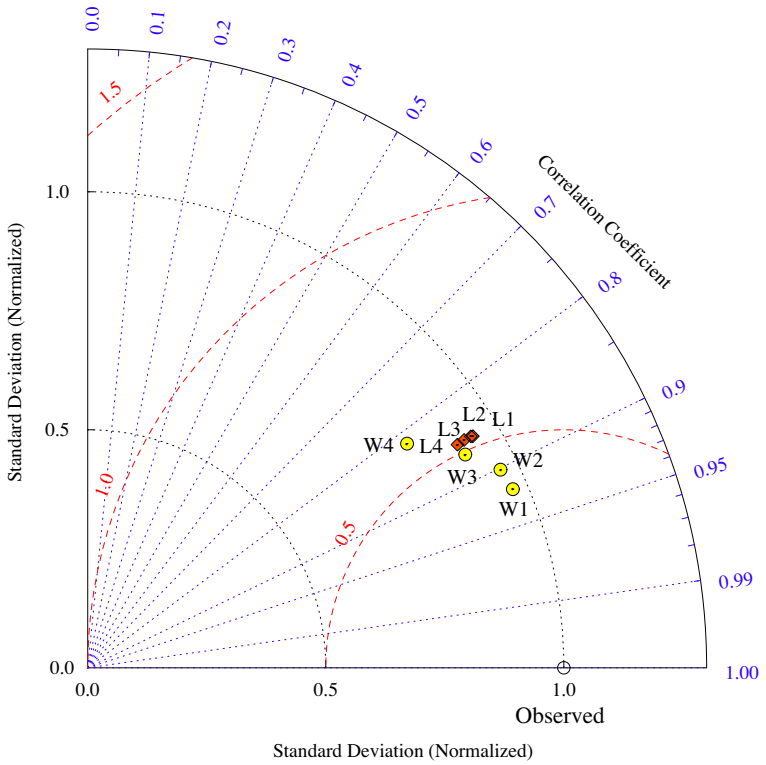

Fig. 6. Taylor diagram as Fig. 4 but displaying a statistical comparison with observation of the means over all stations for each of the four forecast days. The yellow circles refer to the significant wave height (W1, W2, W3, W4) and the red diamonds to the total water level (L1, L2, L3, L4).

The Taylor diagram of Fig. 6 is used to investigate the skill characteristics of both the total water level and the significant wave height predictions for each day of forecast. The average statistics is reported at the bottom of Tables 3 and 4.

The diagram indicates that the model performance worsen with the forecast lead time showing a progressive underestimation of the amplitude of the significant wave height and of the total water level variations. This is more evident for the wave height, with a increase of mean BIAS (from 4 to 15 cm), mean CRMS (from 22 to 33 cm), mean SCI (from 0.33 to 0.48), and a decrease of mean correlation (from 0.92 to 0.82).

In addition to the expected intrinsic increase of forecast error with the forecast validity interval, there is an important decrease of resolution of the predicted wind field (due to the implementation of the meteorological models as described in Section 2.3) after forecast day 2 (and also after forecast day 3) that adversely affects the accuracy of the marine forecast, at least for the area around Italy where the high resolution of the MOLOCH model for the first 48 h period can be fully exploited. The use of high resolution (a few km) wind input over Mediterranean sub-basins, as for example the Adriatic sea, seems therefore to allow avoidance of correcting factors that were applied in the past to amplify the wind speed deriving from relatively low resolution numerical models (Cavaleri and Bertotti, 1997).

The forecast skill of the total water level does not change significantly with validity time. This can be due to the fact that, while the wave dynamics is dominated by the action of the wind alone (in particular local gustiness), the barotropic flow is mostly influenced by the more predictable tidal effect, the piling up due to surface winds, and the atmospheric pressure, which significantly modifying sea level through the inverse barometer effect. In fact, the relative contribution of the mechanical atmospheric forcing (i.e., the atmospheric pressure and wind) along the Italian peninsula explains only half of the total water level variance. Moreover the error of reproducing the tidal signal is constant during the short term forecast, and it is reasonable to assume that the atmospheric pressure field has a smaller variability and is better predicted with respect to the turbulence characteristics of the surface winds.

4. Conclusions

A coupled wave, astronomical tide and storm-surge model has been developed and applied to the Mediterranean Sea on unstructured grid. The third-generation WWMII spectral wave model has been coupled with the 3-D hydrodynamic SHYFEM model. The method used here, and the numerical schemes employed in both models have been successfully tested and showed to be efficient in simulating tides, storm surges and waves along the Italian peninsula. This marine model uses, as atmospheric data input, forecast fields produced by a meteorological model chain, from global to local scale.

The variable resolution of the method and the effect of the depth-varying loading factor lead the present model, at least for the Italian coast and for period of test, to perform better than other tidal models. Tide-surge non-linear interaction turns out to improve significantly the tidal model performance. Moreover, it has been found that the use of a three-dimensional formulation enhances the results of the tide-surge model.

Hindcast results showed that the hydrodynamic-wave model coupling slightly enhanced the wave prediction, while wave effect on the water level could not be resolved properly since the resolution of the numerical mesh of this application is not enough to describe the surf zone along the whole Italian coast.

The modelling system described in this work, which includes meteorological and oceanographic components, represents a powerful short term water level forecasting system for the Italian re-

gion. The high spatial resolution of the Kassandra system along the Italian peninsula, exploiting unprecedented high resolution meteorological model input, allows the detailed description of the sea water level and the wave field. The developed model gives a significant improvement in predicting the total water level along the Italian coastal area and represents a potentially useful tool in bathymetry and altimetry corrections. Even if the forecast skill for the surge signal depends strongly on the range of the forecast, the total water level is less depended on it.

The short term storm surge forecasts of the Kassandra system for the whole Mediterranean are available at http://www.ismar.cnr.it/kassandra. The operational model has been recently implemented also in the Black Sea. The implementation of the baroclinic version of the model and the investigation of different surface wind stress parameterizations will be the subject of future work.

Acknowledgements

The authors thank the Italian Institute for Environmental Protection and Research (ISPRA) for providing water level and wave data. Finally, the authors would like to thank Dr. Luigi Cavaleri for the critical review of the manuscript. This research was partially funded by RITMARE Flagship Project, funded by MIUR under the NRP 2011-2013, approved by the CIPE Resolution 2/2011 of 23.03.2011.

References

Arabelos, D.N., Papazachariou, D.Z., Contadakis, M.E., Spatalas, S.D., 2010. A new tide model for the Mediterranean Sea based on altimetry and tide gauge assimilation. Ocean Sci. Discuss. 7, 1703–1737.

Ardhuin, F., Bertotti, L., Bidlot, J.-R., Cavaleri, L., Filipetto, V., Lefevre, J.-M., Wittmann, P., 2007. Comparison of wind and wave measurements and models in the Western Mediterranean Sea. Ocean Eng. 34 (3–4), 526–541.

Bajo, M., Umgiesser, G., 2010. Storm surge forecast through a combination of dynamic and neural network models. Ocean Modell. 33 (1–2), 1–9.

Bajo, M., Zampato, L., Umgiesser, G., Cucco, A., Canestrelli, P., 2007. A finite element operational model for storm surge prediction in Venice. Estuar Coast Shelf S. 75 (1–2), 236–249.

Battjes, J.A., Janssen, J.P.F.M., 1978. Energy loss and set-up due to breaking of random waves. In: Proceedings 16th International Conference Coastal Engineering, ASCE. pp. 569–587.

Bellafiore, D., Bucchignani, E., Gualdi, S., Carniel, S., Djurdjevi, V., Umgiesser, G., 2011. Evaluating meteorological climate model inputs to improve coastal hydrodynamic studies. Adv. Sci. Res. 6, 227–231.

Bertin, X., Bruneau, N., Breilh, J.-F., Fortunato, A.B., Karpytchev, M., 2012. Importance of wave age and resonance in storm surges: The case Xynthia Bay of Biscay. Ocean Modell. 42, 16–30.

Bertotti, L., Cavaleri, L., 2009. Wind and wave predictions in the Adriatic Sea. J. Marine Syst. 78 (Supplement), S227–S234.

Bertotti, L., Bidlot, J.-R., Bunney, C., Cavaleri, L., Delli Passeri, L., Gomez, M., Lefèvre, J.-M., Paccagnella, T., Torrisi, L., Valentini, A., Vocino, A., 2011. Performance of different forecast systems in an exceptional storm in the Western Mediterranean Sea. Q. J. Roy. Meteor. Soc. 138, 34–55.

Blumberg, A., Mellor, G.L., 1987. A description of a three-dimensional coastal ocean circulation model. In: Heaps, N.S. (Ed.), Three-Dimensional Coastal Ocean Models. American Geophysical Union, Washington, DC, pp. 1–16.

Bolaños, R., Osuna, P., Wolf, J., Monbaliu, J., Sanchez-Arcilla, A., 2011. Development of the POLCOMS-WAM current-wave model. Ocean Modell. 36 (1–2), 102–115.

Bowen, A.J., Inman, D.L., Simmons, V.P., 1968. Wave setdown and setup. J. Geophys. Res. 73, 2569–2577.

Brown, J.M., Wolf, J., 2009. Coupled wave and surge modelling for the eastern Irish Sea and implications for model wind-stress. Continental Shelf Res. 29 (10), 1329–1342.

Brown, J.M., Bolaños, R., Wolf, J., 2011. Impact assessment of advanced coupling features in a tide-surge-wave model, POLCOMS-WAM, in a shallow water application. J. Marine Syst. 87 (1), 13–24.

Burchard, H., Petersen, O., 1999. Models of turbulence in the marine environment – a comparative study of two equation turbulence models. J. Marine Syst. 21, 29–53.

Buzzi, A., Fantini, M., Malguzzi, P., Nerozzi, F., 1994. Validation of a limited area model in cases of Mediterranean cyclogenesis: surface fields and precipitation scores. Meteorol. Atmos. Phys. 53, 137–153.

Cavaleri, L., Bertotti, L., 1997. In search of the correct wind and wave fields in a minor basin. Mon. Weather Rev. 125 (8), 1964–1975.

Cavaleri, L., Bertotti, L., Buizza, R., Buzzi, A., Masato, V., Umgiesser, G., Zampieri, M., 2010. Predictability of extreme meteo-oceanographic events in the Adriatic Sea. Q. J. Roy. Meteor. Soc. 136, 400–413.

Cera, T.B., 2011. Tidal analysis program in python (TAPPY). Retrieved from <http://tappy.sourceforge.net>

Debreu, L., Marchesiello, P., Penven, P., Cambon, G., 2012. Two-way nesting in split-explicit ocean models: algorithms, implementation and validation. Ocean Modell. 49–50, 1–21.

de Vries, H., Breton, M., de Mulder, T., Krestenitis, Y., Ozer, J., Proctor, R., Ruddick, K., Salomon, J.C., Voorrips, A., 1995. A comparison of 2d storm surge models applied to three shallow european seas. Environ. Softw. 10 (1), 23–42.

Drofa, O.V., Malguzzi, P., 2004. Parameterization of microphysical processes in a non hydrostatic prediction model. In: Proceedings 14th International Conference on Clouds and Precipitation (ICCP). Bologna, 19–23 July 2004. pp. 1297–3000.

Eldeberky, Y., 1996. Nonlinear Transformation of Wave Spectra in the Nearshore Zone. Ph.D. thesis, TU-Deft, Delft, the Netherlands.

Foreman, M.G.G., Henry, R.F., Walters, R.A., Ballantyne, V.A., 1993. A finite element model for tides and resonance along north coast of British Columbia. J. Geophys. Res. 98, 2509–2531.

Grant, W.D., Madsen, O.S., 1979. Combined wave and current interaction with a rough bottom. J. Geophys. Res. 84, 1797–1808.

Hasselmann, S., Hasselmann, K., 1981. A symmetrical method of computing the nonlinear transfer in a gravity wave spectrum. Hamb. Geophys. EinzelSchr. A, 52, 138.

Hasselmann, K., Barnett, T.P., Bouws, E., Cartwright, H.C.D., Enke, K., Ewing, J.A., Gienapp, H., Hasselmann, D.E., Kruseman, P., Meerburg, A., Mqller, P., Olbers, D.J., Richter, K., Sell, W., Walden, H., 1973. Measurements of wind-wave growth and swell decay during the Joint North Sea Wave Project (JONSWAP). Tech. Rep. A8(12), Dtsch. Hydrogr Z., 1–95.

Horsburgh, K.J., Wilson, C., 2007. Tide-surge interaction and its role in the distribution of surge residuals in the North Sea. J. Geophys. Res. 112, C08003.

Jones, J.E., Davies, A.M., 2008a. On the modification of tides in shallow water regions by wind effects. Journal of Geophysical Research 113 (C05014), 28pp.

Jones, J.E., Davies, A.M., 2008b. Storm surge computations for the west coast of Britain using a finite element model (TELEMAC). Ocean Dyn. 58 (5–6), 337–363.

Kain, J.S., 2004. The Kain–Fritsch convective parameterization: an update. J. Appl. Meteor. 43, 170–181.

Kantha, L.H., 1995. Barotropic tides in the global oceans from a nonlinear tidal model assimilating altimetric tides 1. Model description and results. J. Geophys. Res.100 (C12), 25, pp. 283–25, 309.

Kantha, L.H., Clayson, C.A., 2000. Numerical models of oceans and oceanic processes. Int. Geophys. 66.

Kim, S.Y., Yasuda, T., Mase, H., 2008. Numerical analysis of effects of tidal variations on storm surges and waves. Appl. Ocean Res. 30 (4), 311–322.

Lane, E., Walters, R., Gillibrand, P., Uddstrom, M., 2009. Operational forecasting of sea level height using an unstructured grid ocean model. Ocean Modell. 28 (1–3), 88–96.

Lionello, P., Sanna, A., Elvini, E., Mufato, R., 2006. A data assimilation procedure for operational prediction of storm surge in the northern adriatic sea. Continental Shelf Res. 26 (4), 539–553.

Longuet-Higgins, M.S., Steward, R.W., 1964. Radiation stresses in water waves; a physical discussion with applications. Deep-Sea Res. 11, 529–562.

Lyard, F., Lefevre, F., Letellier, T., Francis, O., 2006. Modelling the global ocean tides: modern insights from FES2004. Ocean Dyn. 56, 394–415.

Makin, V.K., Stam, M., 2003. New drag formulation in NEDWAM. Tech. Rep. TR-250, KNMI, pp. 16.

Malguzzi, P., Grossi, G., Buzzi, A., Ranzi, R., Buizza, R., 2006. The 1966 century flood in Italy: a meteorological and hydrological revisitation. J. Geophys. Res. 111, D24106.

Marcos, M., Tsimplis, M.N., Shaw, A.G.P., 2009. Sea level extremes in southern Europe. J. Geophys. Res. 144 (C01007), 16.

Marcos, M., Jordà, G., Gomis, D., Pérez, B., 2011. Changes in storm surges in southern Europe from a regional model under climate change scenarios. Global Planet. Change 77 (3–4), 116–128.

Moon, I.-J., Kwon, J.-I., Lee, J.-C., Shim, J.-S., Kang, S.K., Oh, I.S., Kwon, S.J., 2009. Effect of the surface wind stress parameterization on the storm surge modeling. Ocean Modell. 29 (2), 115–127.

Oddo, P., Pinardi, N., Zavatarelli, M., Colucelli, A., 2006. The adriatic basin forecasting system. Acta Adriatica 47 (Suppl), 169–184.

Olabarrieta, M., Warner, J.C., Armstrong, B., Zambon, J.B., He, R., 2012. Ocean-atmosphere dynamics during Hurricane Ida and Nor'Ida: an application of the coupled ocean-atmosphere-wave-sediment transport (COAWST) modeling system. Ocean Modell. 43–44, 112–137.

Øyvind, S., Albretsen, J., Janssen, P.A.E.M., 2007. Sea-state-dependent momentum fluxes for ocean modeling. J. Phys. Oceanogr. 37, 2714–2725.

Richard, E., Buzzi, A., Zängl, G., 2007. Quantitative precipitation forecasting in mountainous regions: the advances achieved by the Mesoscale Alpine programme. Quart. J. Roy. Meteorol. Soc. 133, 831–846.

Roland, A., Cucco, A., Ferrarin, C., Hsu, T.-W., Liau, J.-M., Ou, S.-H., Umgiesser, G., Zanke, U., 2009. On the development and verification of a 2d coupled wave-current model on unstructured meshes. J. Marine Syst. 78 (Supplement), S244–S254.

Sguazzero, P., Giommoni, A., Goldmann, A., 1972. An empirical model for the prediction of the sea level in Venice. Technical Report 25, IBM, Venice Scientific Center.

Smagorinsky, J., 1963. General circulation experiments with the primitive equations, I. The basic experiment. Monthly Weather Review 91, 99–152.

Smith, S., Banke, E., 1975. Variation of the sea surface drag coefficient with wind speed. Q. J. Roy. Meteorol. Soc. 101, 665–673.

Stepanov, V.N., Hughes, C.W., 2004. Parameterization of ocean self-attraction and loading in numerical models of the ocean circulation. J. Geophys. Res. 109, C03037.

Taylor, K.E., 2001. Summarizing multiple aspects of model performances in a single diagram. J. Geophys. Res. 106, 7183–7192.

Tolman, H.L., 1991. A third generation model for wind waves on slowly varying, unsteady and inhomogeneous depths and currents. J. Phys. Oceanogr. 21, 782–797.

Tsimplis, M.N., Proctor, R., Flather, R.A., 1995. A two-dimensional tidal model for the Mediterranean Sea. J. Geophys. Res. 100 (C8), 16, 223–16, 239.

Umgiesser, G., Bergamasco, A., 1995. Outline of a Primitive Equations Finite Element Model. Rapporto e Studi, Istituto Veneto of Scienze, Lettere ed Arti XII, pp. 291–320.

Umgiesser, G., Melaku Canu, D., Cucco, A., Solidoro, C., 2004. A finite element model for the Venice Lagoon. Development, set up, calibration and validation. J. Marine Syst. 51, 123–145.

Wakelin, S.L., Proctor, R., 2002. The impact of meteorology on modelling storm surges in the adriatic sea. Global Planet. Change 32, 97–119.

Walters, R.A., 2006. Design considerations for a finite element coastal ocean model. Ocean Modell. 15 (1–2), 90–100.

Weisberg, R.H., Zheng, L., 2008. Hurricane storm surge simulations comparing three-dimensional with two-dimensional formulations based on an Ivan-like storm over the Tampa Bay, Florida region. J. Geophys. Res. 133 (C12001).

Wolf, J., 2009. Coastal flooding: impacts of coupled wave-surge-tide models. Nat. Hazards 49 (2), 241–260.

Xia, H., Xia, Z., Zhu, L., 2004. Vertical variation in radiation stress and wave-induced current. Coastal Eng. 51, 309–321.

Xing, J., Jones, J.E., Davies, A.M., Hall, P., 2011. Modelling tide-surge interaction effects using finite volume and finite element models of the Irish Sea. Ocean Dyn. 61 (8), 1137–1174.

Young, I.R., Sobey, R.J., 1985. Measurements of the wind-wave energy flux in an opposing wind. J. Fluid Mech. 151, 427–442.

Zampato, L., Umgiesser, G., Zecchetto, S., 2007. Sea level forecasting in Venice through high resolution meteorological fields. Estuar. Coast. Shelf Sci. 75 (1–2), 223–235.

Zhang, Y., Baptista, A.M., 2008. SELFE: A semi-implicit Eulerian–Lagrangian finite-element model for cross-scale ocean circulation. Ocean Modell. 21 (3–4), 71–96.